The Astrophysical Journal, 659:931–940, 2007 April 20

THE ROLE OF GALAXY INTERACTIONS AND MERGERS IN STAR FORMATION AT $z \leq 1.3$: MID-INFRARED PROPERTIES IN THE *SPITZER* FIRST LOOK SURVEY[1]

C. R. Bridge,[2] P. N. Appleton,[3] C. J. Conselice,[4] P. I. Choi,[5] L. Armus,[3] D. Fadda,[3] S. Laine,[3] F. R. Marleau,[3] R. G. Carlberg,[2] G. Helou,[3] and L. Yan[3]

Received 2006 August 20; accepted 2006 December 21

ABSTRACT

By combining the 0.12 deg^2 F814W *Hubble Space Telescope* (*HST*) and *Spitzer* MIPS 24 μm imaging in the First Look Survey (FLS), we investigate the properties of interacting and merging mid-infrared bright and faint sources at $0.2 \leq z \leq 1.3$. We find a marginally significant increase in the pair fraction for MIPS 24 μm detected, optically selected close pairs, with a pair fraction of 0.25 ± 0.10 at $z \sim 1$, in contrast to 0.11 ± 0.08 at $z \sim 0.4$, while galaxies below our 24 μm MIPS detection limit show a pair fraction consistent with zero at all redshifts. In addition, 24 μm detected galaxies with fluxes $\geq$0.1 mJy are on average 5 times more likely to be in a close galaxy pair in the range $0.2 \leq z \leq 1.3$ than galaxies below this flux limit. Using the 24 μm flux to derive the total far-IR luminosity, we find that paired galaxies (early-stage mergers) are responsible for $27\% \pm 9\%$ of the IR luminosity density resulting from star formation at $z \sim 1$, while morphologically classified (late stage) mergers make up $34\% \pm 11\%$. This implies that $61\% \pm 14\%$ of the infrared luminosity density and, in turn, $\sim$40% of the star formation rate density at $z \sim 1$ can be attributed to galaxies at some stage of a major merger or interaction. We argue that close pairs/mergers in a LIRG/ULIRG phase become increasingly important contributors to the IR luminosity and star formation rate density of the universe at $z > 0.7$.

Subject headings: galaxies: evolution — galaxies: formation — galaxies: interactions — galaxies: starburst

Online material: color figure

1. INTRODUCTION

Hierarchical models and observations suggest that galaxy mergers and interactions play a key role in galaxy assembly and star formation, but to what extent is still unclear. Studies of gas-rich mergers in the local universe (e.g., the Antennae; see Schweizer 1982) and *N*-body simulations (Mihos & Hernquist 1996; Barnes 2004) have revealed fundamental signatures of the galaxy merger process, including tidal tails, multiple nuclei, and violent bursts of star formation. While interaction-induced star formation is thought to be primarily responsible for ultraluminous infrared galaxies (ULIRGs; $L_{\rm IR} \geq 10^{12}\,L_{\odot}$) both locally and at high redshift (Sanders et al. 1988; Dasyra et al. 2006), luminous infrared galaxies (LIRGs; $L_{\rm IR} \sim 10^{11}$–$10^{12}\,L_{\odot}$) appear to have multiple driving mechanisms, merger-induced star formation being only one.

Luminous infrared (IR) galaxies are thought to be the dominant producers of the cosmic infrared background and major contributors to the evolution of the cosmic star formation rate (CSFR) of galaxies, especially at $z \geq 0.7$ (Elbaz et al. 2002; Le Floc'h et al. 2005). The rapid decline from $z \sim 1$ of the CSFR density has been linked to a decline in the merger rate. However, recent close pair studies have suggested that the merger rate has remained fairly constant from $z \sim 1$ (Bundy et al. 2004; Lin et al. 2004), and at $z \geq 0.7$ the IR population is dominated by morphologically normal galaxies (Bell et al. 2005; Melbourne et al. 2005; Lotz et al. 2006). The combination of these two results suggest that the bulk of star formation at $z \sim 1$ is not driven by major mergers.

However, it must be noted that different merger selection criteria probe different stages of the merger process. Quantitative measurements of galaxy asymmetry (Abraham et al. 1996a, 1996b; Conselice et al. 2003b) are more likely to probe later stages, while early-stage mergers can be identified by carefully searching for close companions. There should be some overlap between these techniques if galaxy pairs are close enough to have induced strong tidal interactions, but galaxies in pairs could also have normal morphologies; hence, if early-stage mergers are not considered, the impact interactions/merging have will be underestimated.

Traditionally, close pair studies have been carried out in the optical/near-IR (Patton et al. 1997, 2000, 2002; Carlberg et al. 2000; Le Fèvre et al. 2000; Lin et al. 2004; Bundy et al. 2004). However, recent investigations have begun to explore the mid-IR properties (star formation) of galaxy pairs, finding a mid-IR enhancement in pairs separated by less than tens of kpc (Lin et al. 2007). The amount of IR luminosity stemming from individual processes (star formation or fueling an active galactic nucleus [AGN]) in interacting pairs and mergers still remains open. To investigate this question, we have conducted a study of the frequency of MIPS 24 μm detected and undetected close optical galaxy pairs and morphologically defined mergers in the *Spitzer* First Look Survey (FLS).[6] We find that the fraction of 24 μm detected, optically selected close pairs and mergers increases with redshift and are important contributors to the IR luminosity and star formation rate density at $z \sim 1$. In the discussion that follows,

[1] Some of the data presented herein were obtained at the W. M. Keck Observatory, which is operated as a scientific partnership among the California Institute of Technology, the University of California, and the National Aeronautics and Space Administration. The observatory was made possible by the generous financial support of the W. M. Keck Foundation.

[2] University of Toronto, Toronto, ON, Canada, M5S 3H4; bridge@astro.utoronto.ca.

[3] Spitzer Science Center, California Institute of Technology, Pasadena, CA 91125.

[4] University of Nottingham, University Park, NG9 2RD, United Kingdom.

[5] Department of Physics and Astronomy, Pomona College, Claremont, CA.

[6] For details of the FLS observation plan and the data release, see http://ssc.spitzer.caltech.edu/fls.

any calculation requiring cosmology assumes $\Omega_m = 0.3$, $\Omega_\Lambda = 0.70$, and $H_0 = 70$ km s^{-1} Mpc^{-1}.

2. PHOTOMETRIC AND SPECTROSCOPIC OBSERVATIONS

The *Spitzer* extragalatic component of the FLS is a 3.7 deg^2 region centered around R.A. = $17^h18^m00^s$, decl. = $59^\circ30'00''$. Observations of this field were taken using all four Infrared Array Camera (IRAC) channels (Fazio et al. 2004) and three Multiband Imaging Photometer (MIPS) bands (Rieke et al. 2004). Additional ground-based images in u^* and g' from the CFHT MegaCam (Shim et al. 2006) and g' and i' data from the Palomar 200″ LFC and NOAO 4 m R and K' band (Fadda et al. 2004; T. M. Glassman et al. 2007, in preparation) have also been obtained. This work focuses on the 0.12 deg^2 *HST* ACS F814W imaging of the verification strip, which has 3 σ depths in MIPS 24 μm of 0.1 mJy. Object detection and photometry were performed using Sextractor (Bertin & Arnouts 1996). Particular care was taken to ensure accurate deblending of galaxies in close proximity to one another, while avoiding detections of substructure within a single galaxy, consistent with other reductions of *HST* imaging with close galaxy pairs in mind (Patton et al. 2005). There were ~59,000 sources extracted within the F814W$_{AB}$ band (hereafter extracted magnitudes are referred to as "I_{AB}"). We compared our number counts to those from the Hubble Deep Field (HDF) North and South and determined a limiting magnitude of $I_{AB} \sim 27.4$.

Using the full MIPS catalog from the FLS (Fadda et al. 2006), we selected 24 μm sources within the area covered by the ACS imaging (~0.12 deg^2). In order to correlate the MIPS objects with those identified in the optical, we first cross-identified sources from the MIPS 24 μm sample to the IRAC catalog (Lacy et al. 2005) using a tolerance radius of 2.0″. This choice was primarily motivated by the FWHM of the MIPS 24 μm (PSF ~ 6″) and confirmed by visual inspection. We then cross-correlated the IRAC MIPS catalog and the ACS sample, which we band-merged with u^*, g', and R, requiring a positional agreement of $\leq 1''$. When multiple counterparts were identified, we selected the closest object. Ultimately, we found 1155 ACS sources also detected by IRAC and MIPS at 24 μm.

The redshifts used in this study were determined exclusively from optical spectroscopy. They were obtained by cross-correlating the ACS sample, limited to $I_{AB} \leq 26.5$ ($N \sim 29{,}000$) with various FLS spectroscopic data sets. The vast majority of the included redshifts (≥97%) were obtained with the Deep Imaging Multi-Object Spectrograph (DEIMOS) on the W. M. Keck II 10 m telescope; however, the final sample also included a few redshifts based on Sloan Digitized Sky Survey (SDSS) and WIYN Hydra/MOS (F. R. Marleau et al. 2007, in preparation) spectra. Galaxies in the FLS verification region were targeted for spectroscopic follow-up during two DEIMOS campaigns that bracketed *Spitzer*'s launch. The selection criteria for these campaigns are summarized below. For the 2003 prelaunch campaign, targets were selected based on NIR (K_s) and optical (g, R, and i) colors. The primary sample included sources with $K_s < 20.2$ and $R > 19.0$ and a (g, R, and i) color selection that restricted the numbers of low-redshift ($z \leq 0.6$) sources. For the 2004 postlaunch campaign, a purely 24 μm selected sample ($f_{24} > 120$ μJy) was targeted for follow-up. The combined I_{AB} distribution of targeted and detected sources is shown in Figure 1 (*top*), along with the cumulative redshift identification efficiency (*bottom*). The overall spectroscopic completeness (defined here as the fraction of targeted sources with high-quality redshifts) is ~70% for the full sample and ~80% for sources with $I_{AB} < 25.0$. For a more detailed description of the observing strategy, primary selection criteria, and the overall flux and redshift distributions, see Choi et al. (2006).

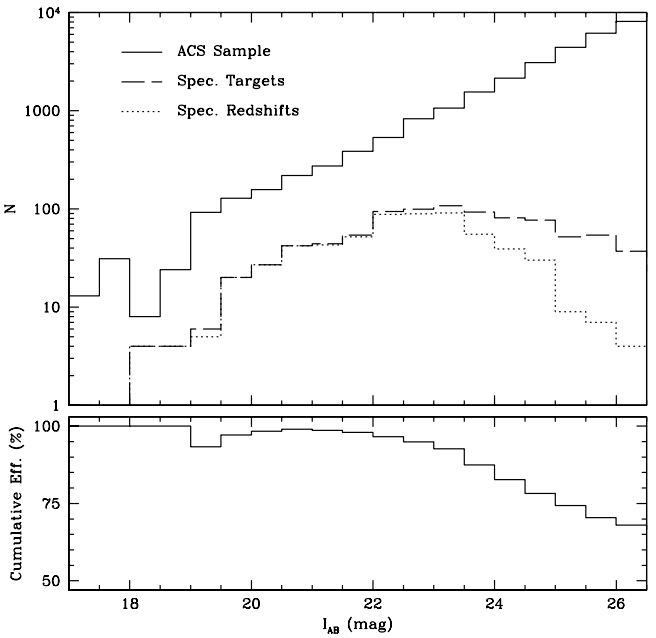

FIG. 1.— *Top*, I_{AB} mag distribution for the FLS sample (*solid line*), the sample targeted for spectroscopy (*long-dashed line*), and those for which spectroscopic redshifts were acquired (*dotted line*); *bottom*, cumulative redshift identification efficiency. The overall spectroscopic completeness is ~70% for the full sample and ~80% for sources with $I_{AB} < 25.0$.[*See the electronic edition of the Journal for a color version of this figure.*]

Since we were exploring the mid-IR properties of galaxies, no optical limit was imposed; instead, an IR luminosity cut ($L_{IR} \geq 5.0\times10^{10}$ or 1.0×10^{11} $L_\odot$) was used, so that a fair comparison could be made at different redshifts. The absolute B magnitude (M_B) distribution of the MIPS spectroscopic sample in the interval $0.5 < z < 1.3$ probes $-21 \leq M_B \leq -19$ fairly uniformly, and we are not strongly biased at higher redshifts.

Cross-correlation of the band-merged photometric catalogs with the redshift samples results in a data set of 476 sources with $I_{AB} < 26.5$ and $0.2 \leq z \leq 1.3$. Of those, 245 (51%) are MIPS 24 μm detected with a measured $L_{IR} \geq 5.0\times10^{10}$ $L_\odot$. The remaining 231 (49%) are not detected at 24 μm. Despite the fact that the MIPS and non-MIPS galaxies were selected slightly differently, the resultant colors of objects with spectroscopic redshifts have uniform color properties (Fig. 2).

3. STATISTICS OF CLOSE PAIRS AND MERGERS

To properly constrain the role interactions and mergers play in galaxy evolution, all stages of the process must be considered. Typically, merger history analyses utilize either pair or structural methods. Galaxies in pairs are premergers, or systems undergoing interactions, while morphological or structural methods find galaxies that have already undergone a merger and are dynamically relaxing. When discussing the pair fraction and inferred merger rates (as defined in § 4), it must be noted that these measurements are highly dependent on the techniques and selection criteria used to identify ongoing mergers, especially for galaxies at high redshifts.

The first method, which we call the "close pair method," counts the number of galaxy pairs within some projected separation, r_{proj}, and magnitude difference (Δm). If we assume that these systems will merge within a given timescale due to dynamical friction,

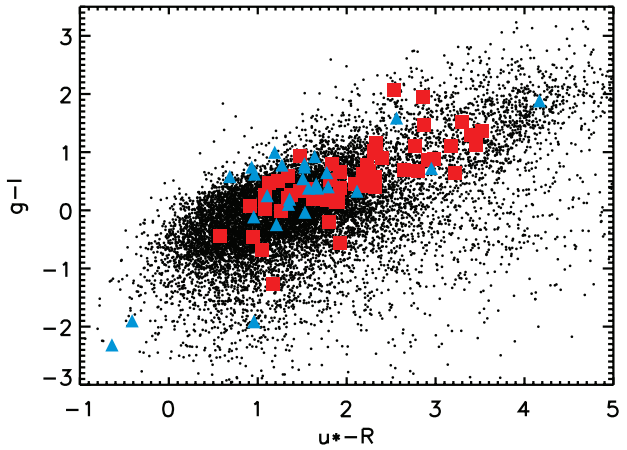

FIG. 2.—Color-color plot. Red squares depict the 24 μm detected objects with spectroscopic redshifts, while blue triangles show the undetected 24 μm spectroscopic sample. The black dots represent the full FLS-ACS catalog for comparison. The 24 μm detected and undetected spectroscopic samples occupy the same color space. Some objects were not detected in all four bands, due to the field coverage, depth, and seeing differences between filters.

we can determine the merger rate. Although not all pairs will merge, they can trigger star formation through gravitational interactions. An alternative is to select merging systems based on morphological indicators, either by overall appearance (Le Fèvre et al. 2000) or computational measurements such as asymmetry (A) and clumpiness (S) of a system (Conselice et al. 2000, 2002; Conselice 2003), Gini coefficient (G), and M_{20} parameters (Abraham et al. 2003; Lotz et al. 2006). Due to the comparatively limited spatial resolution of *Spitzer* (compared with optical imaging), searching for close galaxy pairs or morphological signatures of interaction at mid-IR wavelengths is currently restricted to the nearby universe. However, we can correlate optically selected pairs/mergers with global mid-IR properties and investigate the IR activity in these systems out to high redshifts.

3.1. *Pair Statistics*

We applied the close pairs technique to identify the average number of close companions per galaxy, hereafter N_c. This measurement is similar in nature to the pair fraction when triples or higher order N-tuples are infrequent. Since this is the case here, N_c will occasionally be referred to as "the pair fraction." Companions were selected using a standard operational close pair definition of 5 h^{-1} kpc $\leq r_{\rm proj} \leq$ 20 h^{-1} kpc and an optical magnitude difference, Δm, $\leq$1.5 compared to the host galaxy, thus selecting nearly equal-mass major mergers. The terms "host galaxy" or "primary galaxy" galaxy are both used to refer to the pair member with a measured redshift. The inner radius is applied to avoid detection of substructure within a galaxy, while the outer 20 h^{-1} kpc limit represents the radius within which satellites are expected to strongly interact with the halo of the host and merge within 0.5–0.9 Gyr (Patton et al. 1997; Conselice et al. 2003a). We find 87 close pairs out of 476 galaxies that satisfy these criteria (see Table 1).

To study the fraction of IR-bright galaxies in pairs, we split the pair sample into two subsets, those that were detected and those that were undetected with MIPS at 24 μm down to the flux limits of our survey (0.1 mJy). Figure 3 shows a subset of close pairs (both detected and undetected at 24 μm) with MIPS contours. Due to the small separations of close pairs (20 h^{-1} kpc corresponds to 3.6″ at $z \sim 1$) relative to the beam of the MIPS 24 μm images (FWHM $\sim$ 6″), there are a few instances (five) where only a single 24 μm detection is found centered between the pair members (see the middle left image in Fig. 3). In these cases we assume that all 24 μm flux is coming from the primary galaxy.

3.2. *Field Correction*

Since we have redshift information for only the primary galaxy and not the companions, we need to consider what fraction of these close pairs are a result of random projection effects. A field correction was determined using two separate methods to account for these close pairs. The first assumed the same optical magnitude and redshift distributions independently for both the detected and undetected 24 μm samples, while the positions were randomized. The close pair algorithm was applied to 50 realizations of these mock catalogs, and the average N_c for each redshift bin was taken to be the pair fraction expected from a random distribution. This assumes the absence of clustering.

We investigated the environments of 24 μm detected and undetected objects on scales of $r_{\rm proj} \lesssim 20\ h^{-1}$ kpc and found them to be comparable, confirming that the increase in pair fraction of the 24 μm detected pairs is not because they preferentially lie in clusters. On the other hand, there is a weak indication that galaxies

TABLE 1
FLS CLOSE PAIR STATISTICS

z	$N_{\rm gal}$	N_c^D	N_c^R	N_c	κ
24 μm Detected					
0.2–0.5	32	0.188 (6)	0.078 (2.5)	0.110 ± 0.083	0.83
0.5–0.80	82	0.171 (14)	0.057 (4.7)	0.114 ± 0.040	0.93
0.80–1.0	82	0.122 (10)	0.029 (2.4)	0.093 ± 0.038	0.90
1.0–1.3	49	0.429 (21)	0.182 (8.9)	0.247 ± 0.086	0.67
24 μm Undetected					
0.2–0.5	44	0.136 (6)	0.102 (4.5)	0.034 ± 0.052	1.00
0.5–0.80	76	0.132 (10)	0.134 (10.2)	0 ± 0.039	1.00
0.80–1.0	56	0.214 (12)	0.193 (10.8)	0.021 ± 0.064	0.83
1.0–1.3	55	0.145 (8)	0.180 (9.9)	0 ± 0.065	0.75

NOTES.—$N_{\rm gal}$ is the number of galaxies with a spectroscopic redshift and N_c^D is the number of companions per host fulfilling our pair criteria, while N_c^R is the number of projected companions per host from the field. The corrected fraction of companions per host is given as $(N_c^D - N_c^R)/N_{\rm gal}$, with errors being determined using a jacknife technique. Numbers appearing in parentheses refer to the number of close pairs in the respective redshift bins. "Undetected at 24 μm" refers to sources below the limits of our survey (0.1 mJy). The constant κ is the fractional number of mergers per host galaxy. A $L_{\rm IR} \geq 5.0 \times 10^{10}$ limit was imposed.

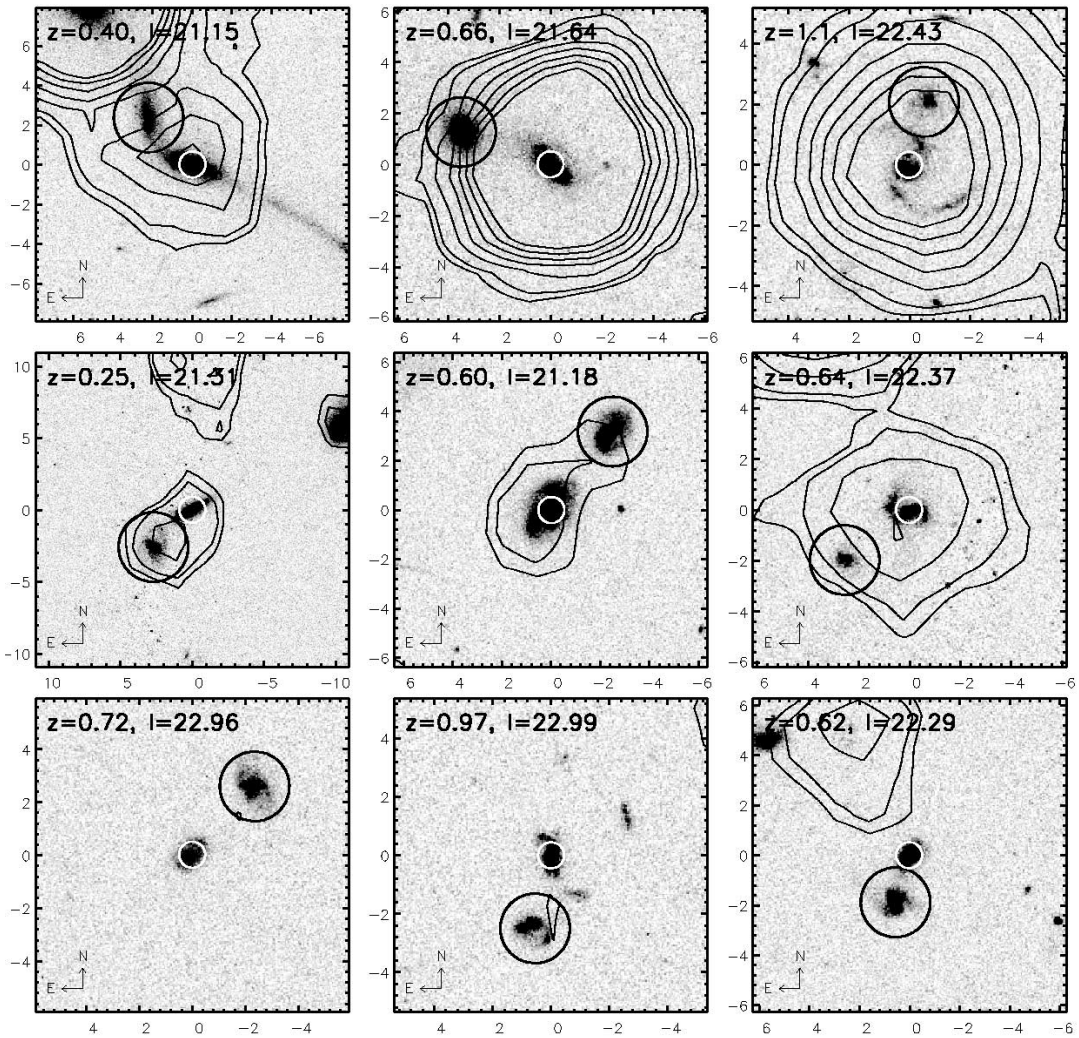

FIG. 3.—Subset of paired galaxies in our sample. Each image is 60 h^{-1} kpc on a side, with axes in arcseconds, centered on the pair member with the spectroscopic redshift also referred to as the "primary" or "host pair member" (*white circle*), while the companion is highlighted in a black circle. The two upper rows include close pairs that were detected at 24 μm, while the lower row is from the undetected 24 μm paired sample. The 3–10 σ 24 μm flux contours are overlaid. The labels show the spectroscopic redshift and I_{AB} magnitude of the primary galaxy.

detected at 24 μm are more likely to lie in small groups. Since such groups may, in some cases, be physical associations, we count such cases as separate pairs. However, the number of these cases is small and does not influence our results in any significant way. The second method utilizes the I_{AB} magnitude distribution of the full photometric catalog (~59,000 sources) and determines the average number of companions within 1.5 mag (I_{AB}), normalized to the area covered by 5 h^{-1} kpc $\leq r_{proj} \leq$ 20 h^{-1} kpc. The results obtained from the two field correction methods agreed within ~2%, which is negligible compared to the uncertainly in N_c. The average of the two methods was taken to be the final field correction. Both the pair catalog and randomly generated catalogs were visually inspected for false pairs due to single galaxies being broken up into multiple components in the source extraction phase or due to contaminating stars in the photometric catalog and were removed.

3.3. *Pair Fractions*

The field-corrected optical pair fractions for the 24 μm detected and undetected subsamples are presented in Figure 4 and Table 1. Errors are computed using the jackknife technique (Efron & Tibshirani 1986); e.g., given a sample of N galaxies, the variance is given by $[(N-1)/N \sum_i \delta_i^2]^{1/2}$. The partial standard deviations, δ_i, are computed for each object by taking the difference between N_c, the quantity being measured, and the same quantity with the ith galaxy removed, N_{ci}, such that $\delta i = N_c - N_{ci}$.

To allow a more direct comparison to be made between the generally lower luminosity low-z pairs and those at higher redshift, we derived pair fractions for MIPS-detected galaxies with $L_{IR} \geq 5.0 \times 10^{10}$ (approximately the IR luminosity of the famous Antennae galaxies). In this way, we ensure that the subluminous galaxies do not strongly influence the pair fractions in the lowest redshift bin. The derived N_c for 24 μm detected close pairs is ~11% ± 8% at $z \sim 0.4$ and increases to 25% ± 10% at $z \sim 1$. In contrast, close pairs with no 24 μm detection show no increase with redshift and have pair fractions consistent with zero at all redshifts. The higher pair fraction of MIPS-bright sources is marginally significant due to the small number of sources in the highest redshift bin; more MIR-selected samples between $z = 1$ and 1.5 are required to strengthen our findings.

We would like to be able to rule out the possibility that N_c is biased by the brightest IR sources at $z \geq 1$, since merger fractions change as a function of luminosity and mass (Conselice et al. 2003b; Xu et al. 2004). To address this issue, we placed a higher

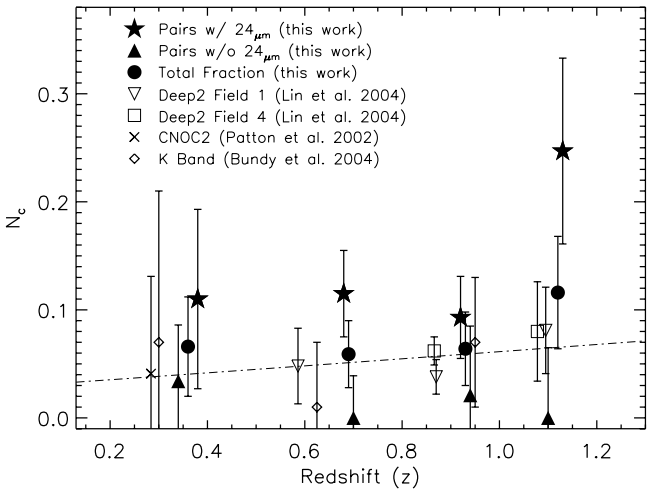

FIG. 4.—Field-corrected pair fraction N_c as a function of redshift as measured in the optical and IR. The stars represent the measurement from our 24 μm detected sample, filled triangles depict the field-corrected pair fraction of the undetected 24 μm subset, and filled circles show the combined pair fraction of the two samples. Other optically determined pair fractions appear as squares (DEEP2 Field 1), open triangles (Field 2; Lin et al. 2004), and a cross (CNOC2; Patton et al. 2002), while the dashed line shows their best power-law fit of $(1+z)^m$ ($m = 1.08 \pm 0.40$). The near-IR pair fraction determined by Bundy et al. (2004) is shown by diamonds. Errors for this work are derived using jacknife statistics, while the IR pair fraction errors, implemented counting statistics, and DEEP2 and CNOC2 errors are determined via bootstrapping. A $L_{\rm IR} \geq 5.0\times10^{10}$ limit was imposed on the 24 μm detected close pairs. Note that each work imposes a slightly different luminosity and stellar mass limit.

IR luminosity limit ($L_{\rm IR} \geq 7.0\times10^{11}$) on the sample, so that at $z \geq 0.7$ the same populations were being probed (we are optically probing $-22 \lesssim M_B \lesssim -19$). We still find an increase in N_c from the lower ($0.8 \leq z \leq 1.0$) to the higher ($z \geq 1$) redshift bins of similar magnitude compared to when the lower IR limit ($L_{\rm IR} \geq 5.0\times10^{10}$) was used. Therefore, the increase in N_c found at $z \geq 1$ is likely not a result of merely probing brighter IR systems, but rather due to a physical increase in the merge rate for the 24 μm population; however, deeper 24 μm imaging and spectroscopy are required to confirm this. When we consider the averaged pair fraction over $0.2 \leq z \leq 1.3$ for the 24 μm detected sample, we find that galaxies above a flux limit of 0.1 mJy are 5 times more likely to be in a close galaxy pair than those below this limit.

3.4. *Morphological Mergers*

To explore the structural components of galaxies in our sample, we used the CAS (concentration, asymmetry, and clumpiness) quantitative classification system (Conselice 1997, 2003a; Conselice et al. 2000, 2002) and visual classifications. To measure the merger fraction using structural classifications, we visually inspected the full 24 μm detected spectroscopic catalog with the following groupings: early types (E and S0), midtypes (Sa-Sb), late types (Sc-Irr), compact systems, disturbed disks, and mergers. The methodology for carrying out this classification is described in detail in Conselice et al. (2005). Basically, each galaxy was viewed on a computer screen and classified into one of our types. Overall, we find that 55% $\pm$ 5% of 24 μm detected galaxies are disks, which is consistent with Bell et al. (2005) and Lotz et al. (2006), while 26% $\pm$ 5% are merging systems and $\sim$6% were classified as disturbed disks and are possible minor mergers. A fraction of the disk-dominated objects do show some visual signs of a morphological disturbance or are in a pair, as we discuss later in this paper.

Galaxies undergoing a major merger event can also generally be identified by their large asymmetries in the rest-frame optical (Conselice et al. 2000, 2003b). We defined a major merger as a galaxy having an asymmetry $A \geq 0.35$ and $I_{\rm AB} \leq 26.5$ (see Fig. 5 for examples). This limit has been shown to be a clean way to find galaxy mergers without significant contamination from nonmerging galaxies (Conselice 2003). Figure 6 shows how the merger fraction for CAS-defined mergers evolves as a function of redshift for both 24 μm detected objects (*top*) and LIRG/ULIRG galaxies (*bottom*). As with the 24 μm detected close pair sample, there is an elevated merger fraction compared to other works (Cassata et al. 2005; Lotz et al. 2006) in which no 24 μm flux limit was imposed, and a slight indication of evolution with redshift, but it is statistically consistent with $m \sim 1.0$ (*dashed line*), where m is the slope of a power law of the form $(1+z)^m$, later discussed in § 5.

We also performed a CAS analysis of our close pairs sample, which revealed that 24 μm detected pairs are notably more asymmetric than the undetected MIPS close pairs (Fig. 7), suggesting that interactions and collisions may play a role in their IR activity. If the 24 μm detected close pairs were generally of a different morphological classification than those pairs undetected at 24 μm, the discrepancy in the asymmetries could be explained. To address this issue, each close pair was visually inspected and classified by four of the authors to be either disk or bulge dominated. We find that 81% of the 24 μm pairs have disk morphologies, while 74% of the undetected 24 μm hosts were also disk dominated; hence, the discrepancy between the asymmetries of the two groups is not caused by classification differences, but rather is a physical effect.

4. MERGER RATES

One of the goals of studying mergers and interactions is to determine how the galaxy merger rate evolves with redshift. Most studies of galaxy mergers involve determining the merger fraction, yet the merger rate, which is defined as the number of galaxies merging per unit time per unit volume, is a more physical quantity that can be used to determine the full merger history. The rate at which galaxies merge also affects the mass function of galaxies and is likely linked to the cosmic star formation rate. Since we are considering a very broad range in the merger process, from early stage or premergers selected via close galaxy pairs and later stage mergers chosen based on morphological criteria, we must be careful when determining their respective merger rates, as the timescales for these processes are all different.

There are two versions of the merger rate definition. The first is the number of mergers that a galaxy will undergo per unit time ($\mathcal{R}_{\rm mg}$), and the second is the total number of mergers taking place per unit time per unit comoving volume ($\mathcal{R}_{\rm mg}$). Since we are primarily interested in mergers that are also mid-IR–bright systems, we will have to restrict ourselves to measuring $\mathcal{R}_{\rm mg}$, because the evolution of the 24 m luminosity function with redshift is currently not well constrained, and our redshifts are not complete enough to reconstruct this evolution.

In order to determine $\mathcal{R}_{\rm mg}$ we need to identify systems that are destined to merge. We have approached this measurement from three different perspectives, close pairs to select premergers or interactions, visual inspection to select interactions after the first passage, and late-stage mergers, as well as CAS criteria that quantitatively select for later stage mergers. By combining information about the number of ongoing mergers (N_m) and the timescales

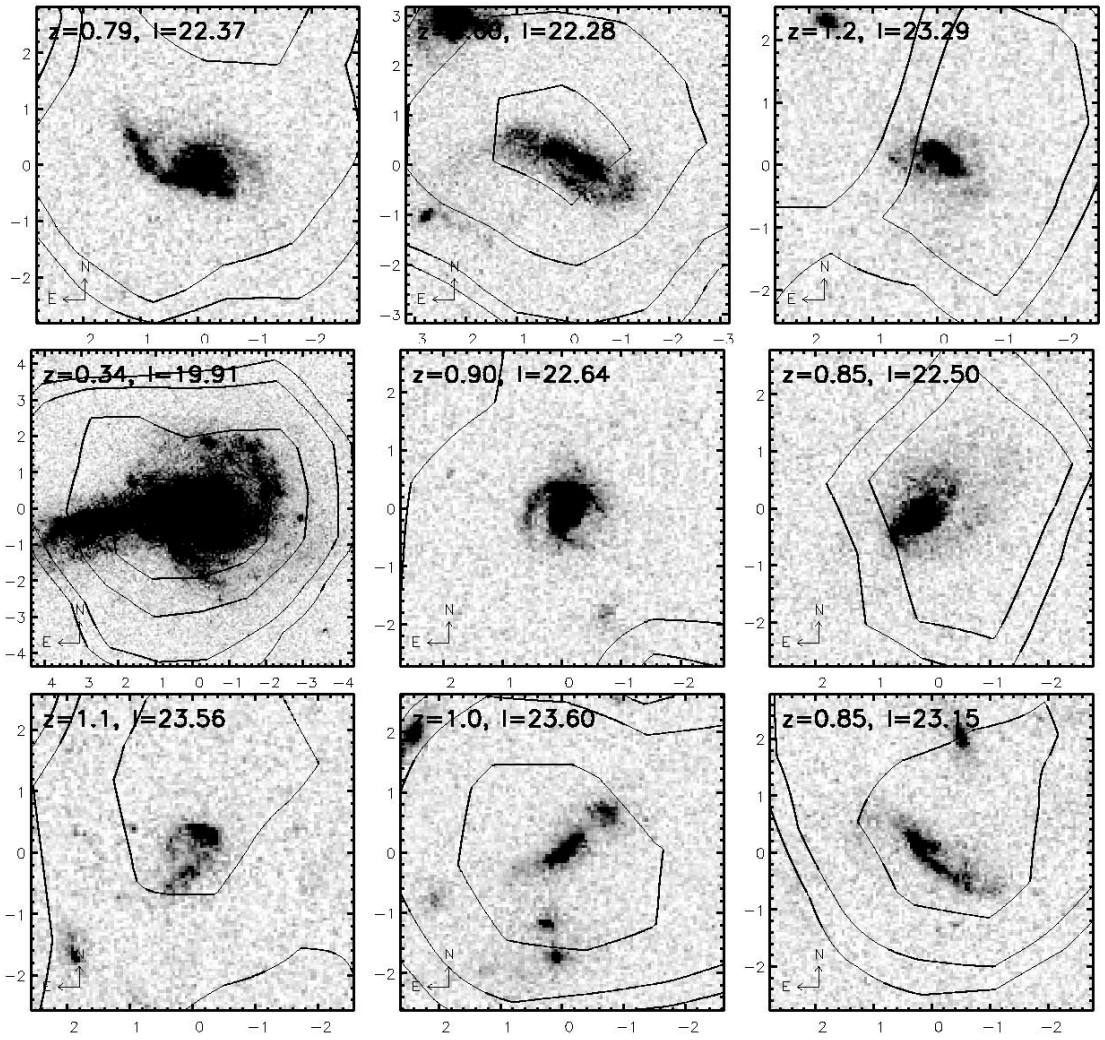

FIG. 5.—Subset of 24 μm detected galaxies in our sample classified as a merger. Each image is 30 h^{-1} kpc on a side, with axes in arcseconds. The 3–10 σ 24 μm flux contours are overlaid. The labels indicate the spectroscopic redshift and F814W$_{AB}$ magnitude.

(T_{mg}) on which they will undergo the merger, one can estimate an overall merger rate $\mathcal{R}_{mg} = N_m/T_{mg}$. Each method of identifying mergers/interactions is capturing a different snapshot of the merger process, each with different merger timescales.

The value of N_c is directly proportional to the number of mergers per galaxy (N_m), such that $N_m = \kappa N_c$ (κ is a constant relating to the number of mergers per galaxy). Hence, the merger rate determined using close galaxy pairs is given by $\mathcal{R}_{mg} = \kappa N_c/T_{mg}$. The value of κ depends on the nature of the merging systems under consideration. If one were to identify a pure set of galaxy pairs, each consisting of one companion undergoing a merger, then $\kappa = 1.0$. In our case, it exclusively accounts for close pairs that are in doubles and perhaps higher order N-tuples. Our definition of κ differs by a factor of 2 from the value in Patton et al. (2000), which in this instance would be $\kappa = 0.5$, since they have redshifts for both pair members and one merger is made up of two companions. We have redshift information for only one pair member; therefore, one merger is made up of a primary and one companion. The merger rate equation for merging galaxies selected by visual classification and CAS parameters is simply $\mathcal{R}_{mg} = f_{mg}/T_{mg}$, where f_{mg} is the galaxy merger fraction.

Before the merger fraction can be used to calculate the merger rate, we need to understand the timescale in which a merger occurs. Each technique of identifying mergers has a different timescale, since each is sensitive to a different interval of the merger process. There are two main methods that have been used to estimate the timescale of a merger: dynamical friction arguments and N-body models. The details of these methods are beyond the scope of this paper, but see Patton et al. (2000) and Conselice (2006) for a review. We take the average merger timescale for a set of close companions of roughly equal mass to merge as $\sim 0.5 \pm 0.25$ Gyr, derived from dynamical arguments (Patton et al. 2000; Conselice 2006). Conselice (2006) showed through N-body simulations that visual classification selects ongoing mergers over a longer timescale (1.0 ± 0.25 Gyr), since the human eye detects both early and later stage mergers, while the asymmetry of a galaxy is sensitive to 0.41 ± 0.17 Gyr (Conselice 2006) of the merger sequence.

5. THE EVOLUTION OF THE GALAXY MERGER RATE $0.2 \leq z \leq 1.3$

Within the past two decades, numerous studies have been performed to estimate the evolution of the galaxy merger fraction, using both the close pair technique (Zepf & Koo 1989; Burkey et al. 1994; Carlberg et al. 1994; Yee & Ellingson 1995; Patton et al. 1997, 2000; Le Fèvre et al. 2000; Lin et al. 2004; Bundy et al. 2004) and morphological parameters (Le Fèvre et al. 2000; Conselice et al. 2003b; Lavery et al. 2004; Lotz et al. 2006). Evolution in

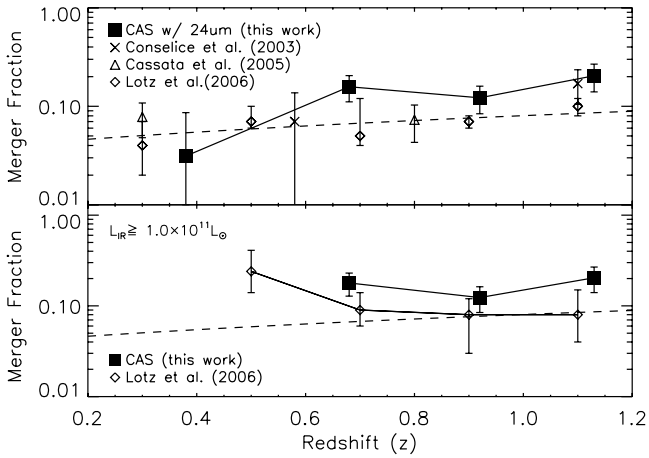

FIG. 6.—Merger fraction as a function of redshift, using quantitative morphological criteria. The squares represent measurements from FLS (this work) of sources with a 24 μm detection. The crosses mark the results of Conselice et al. (2003b), triangles depict those of Cassata et al. (2005), and diamonds represent those of Lotz et al. (2006). *Top*: Merger fraction of other studies with no 24 μm criteria imposed, while the measurements from this work are mergers with $L_{IR} \geq 5.0\times10^{10}\ L_\odot$. The dashed lines show the best fit of $(1+z)^m$ using all points (from the other studies), with no MIPS limit imposed ($m = 1.08$). *Bottom*: Merger fraction for LIRG/ULIRG galaxies ($L_{IR} \geq 1.0\times10^{11}\ L_\odot$). Error bars were derived using Poisson statistics.

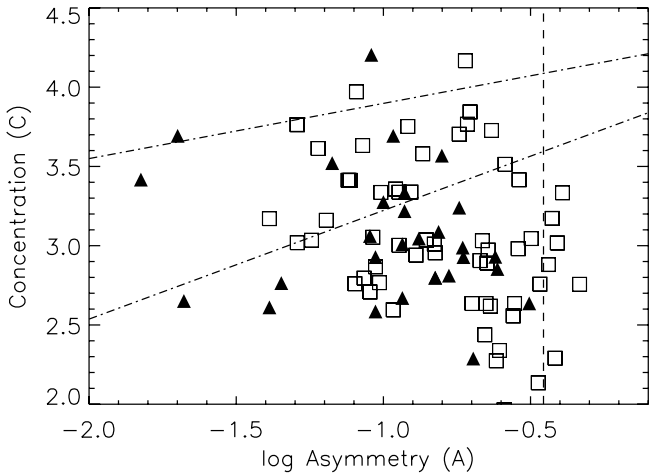

FIG. 7.—Asymmetry-concentration diagram for the 24 μm detected close pairs (*squares*) and undetected pairs (*triangles*). The long-dashed vertical line separates merging and nonmerging systems ($A \geq 0.35$ is considered a merger), while the dash-dotted lines separate early type (*top*) and mid- to late-type (*bottom*) galaxies defined by Conselice (2003). Generally, close pairs are mid/late-type galaxies, and some would also be morphologically classified as mergers.

the galaxy merger fraction is often parameterized by a power law of the form $(1+z)^m$ and has yielded a wide range of results, spanning $0 \lesssim m \lesssim 5$. The large spread in values is in part due to the different selection criteria used to identify merging systems and biases from optical contamination or redshift completeness. Patton et al. (1997) considered these biases and demonstrated that most results to that date were consistent with their estimate of $m = 2.9 \pm 0.9$. Recently, optical and near-IR close pair studies (Lin et al. 2004; Bundy et al. 2004) have derived merger fractions with little redshift evolution ($m \sim 1$), as have some morphological studies using (G) and M_{20} (Lotz et al. 2006).

When we consider all the close pairs identified in our sample, both those detected at 24 μm and those not, we find a merger fraction and rate consistent with recent studies showing little redshift evolution. However, when we separate the pair sample into systems with a 24 μm detection above 0.1 mJy and those below it, we do see a stronger evolution of N_c with redshift (recall that $N_c \propto \mathcal{R}_{\rm mg}$) and therefore also in the merger fraction and rate (Fig. 8). Similarly, visually classified mergers and those identified via asymmetry levels ($A \geq 0.35$) using the CAS parameters also show redshift evolution in the merger fraction and rate. The merger fractions computed using the different methods are in good agreement when normalized by their respective timescales, reinforcing the idea that we are probing different phases of the merger process. Considering all three merger selection techniques, we find the best fit of the merger rate parameterized by $\mathcal{R}(0)(1+z)^m$ to be 0.077 ± 0.045, 2.12 ± 0.93, with a reduced $\chi^2 = 0.39$. This result suggests that when one considers a sample of close galaxy pairs solely on optical fluxes brighter than $M_B = -19$, little evolution of the merger rate with redshift is found. However, galaxies emitting 24 μm flux exhibit an increase in the merger rate with redshift. The infrared luminosity limit ($L_{IR} \geq 10^{11}\ L_\odot$) imposed on the close pairs and mergers allows us to primarily probe systems in a LIRG/ULIRG phase at $z \geq 0.4$ (see § 6 for details). The increase of the merger fraction and rate of this population of galaxies coupled with the fact that LIRG galaxies dominate the CSFR density at $z \geq 0.7$ (Le Floc'h et al. 2005) suggests that merging does in fact play an increasingly important role in star formation out to $z \sim 1$.

6. TOTAL INFRARED LUMINOSITIES OF MERGERS

One way to quantify the role merging galaxies play in triggering star formation is to investigate their contribution to IR luminosity densities. Infrared luminosities (8–1000 μm) were calculated utilizing the 24 μm fluxes and two different template methods (Chary & Elbaz 2001; Dale et al. 2001) in a similar manner to Le Floc'h et al. (2005) for the full MIPS 24 μm spectroscopic sample (Fig. 9). MIPS pairs and mergers share a luminosity distribution similar to 24 μm bright field galaxies, although red AGNs seem generally more luminous, which is in part due to template mismatches (Chary & Elbaz 2001).

The L_{IR} of a galaxy is a combined measure of the reprocessed UV photons intercepted by dust from massive young stars and

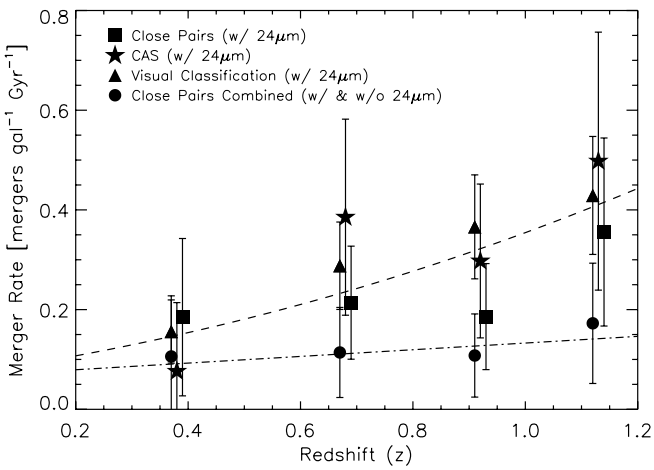

FIG. 8.—Number of mergers per galaxy ($L_{IR} \geq 5\times10^{10}$) as a function of redshift. Three merger/interaction selection techniques are applied, close pairs (*squares*), CAS criteria (*stars*), and visual classification (*triangles*), while merger rates for the combined set (with and without 24 μm detections) using the close pairs method are shown with circles. The long-dashed curve is the best fit of the form $(1+z)^m$, using the FLS data for the three techniques; the dot-dashed curve represents the best fit for the combined total close pairs (MIPS and non-MIPS pairs).

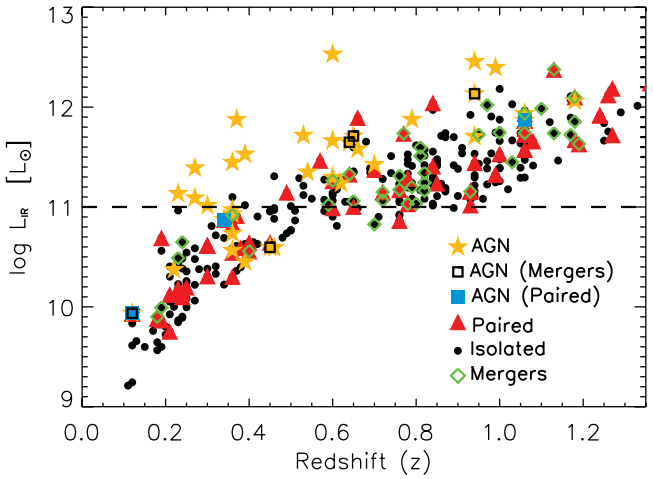

FIG. 9.—Infrared luminosity $L_{IR\ (8-1000\ \mu m)}$ vs. redshift for the MIPS 24 μm sample with spectroscopic redshifts, broken down into galaxies in a close pair (*red triangle*), CAS mergers (*green diamonds*), AGN candidates (*yellow star*), AGN candidates in a close pair (*blue square*), AGN mergers (*open square*), and field galaxies (*black circles*). LIRGs lie above the horizontal dashed line at $L_{IR} \geq 10^{11}\ L_\odot$.

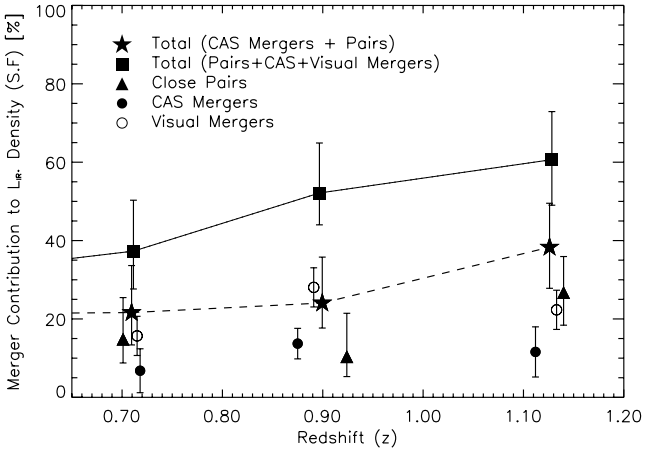

FIG. 11.—Fraction of L_{IR} density (as a result of star formation) as a function of redshift coming from LIRG/ULIRG galaxies in a close pair (premerger phase; *triangles*) or more advanced stage mergers defined morphologically (*circles*). The star symbol indicates the total combined contribution from close pairs and CAS mergers, while squares depict the total from close pairs, CAS, and visually classified mergers. Note that an infrared limit of $L_{IR} \geq 10^{11}\ L_\odot$ was imposed.

AGNs. Therefore, to investigate the contribution an interacting or merging galaxy makes toward the total L_{IR} density from star formation alone, we must first remove AGNs from our sample. Due to the nonuniform rest-frame spectral coverage of our sample, we rely on the four-band IRAC color selection used by (Lacy et al. 2004) to identify and remove AGN candidates (Fig. 10). Over the modest redshift range of our sample, this method is still effective at separating IR-warm AGNs from starburst systems. We find an AGN contamination rate of ~12% for the full 24 μm sample, while ~14% of the hosts in a pair or merger were characterized as AGNs.

With AGN candidate objects removed, we can infer the contribution to the L_{IR} density from star formation coming from 24 μm galaxies in an interaction/merger as a function of redshift. We derive the number of statistically "real" galaxy pairs from our pair fraction result at each redshift interval and determine the total L_{IR} density from close pairs, which is in turn divided by the L_{IR} density from the whole sample. We find that paired galaxies

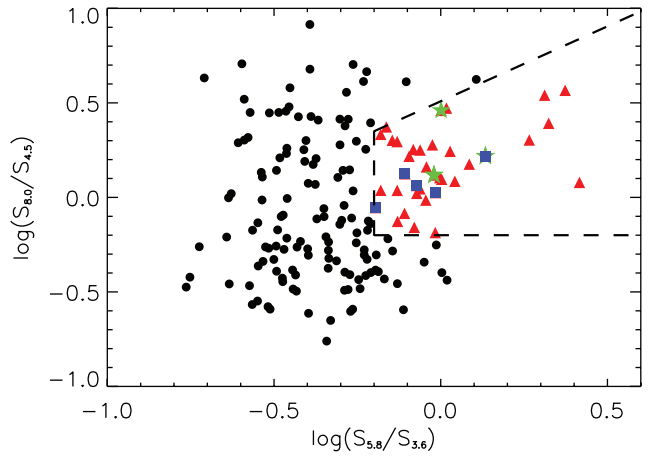

FIG. 10.—IRAC color-color plot using the region in the FLS covered by the ACS imaging. Circles represent objects with spectroscopic redshifts and detections in all four IRAC channels. The red triangles indicate objects that have met the color criteria (*dashed line*) of an AGN candidate (Lacy et al. 2004). The green stars and blue squares depict objects in, respectively, a close galaxy pair or merger whose host was also flagged as an AGN candidate.

($L_{IR} \geq 10^{11}\ L_\odot$) are responsible for 27^{+9}_{-8}% of the IR background stemming from star formation at $z \sim 1$. Since we only know the redshift of the host galaxy, we select "real" close pairs in a statistical sense and derive error bars for the close pair contribution by the spread of 50 realizations of the L_{IR} density from different combinations of 24 μm galaxy pairs. We also applied this analysis to CAS and visually classified mergers, which make up an additional ~12% and ~22% of the IR luminosity density, respectively. Naturally, there is some overlap in mergers identified through close pair criteria and morphological parameters, since interacting pairs can exhibit tidal tails and asymmetric structures, causing them to be identified morphologically as mergers also. We found that 37% of CAS defined mergers were also in a close pair, and 31% of visually identified mergers were also classified by CAS as merging. In cases where a merging system was identified using multiple techniques, its contribution was counted only once. For example, if a merger identified morphologically (either through CAS or visual inspection) is also in a close pair, it is removed from the morphological merger catalog, or if a CAS merger is also identified visually, the merger is removed from the visual merger catalog. This ensures that no close pair or merger is counted more than once when deriving the contribution from interactions and mergers to the IR luminosity density.

The combination of these three merger selection techniques identifies a large range in the merger process, from premerger to late-stage mergers, implying that ~60% of the infrared luminosity density at $z \sim 1$ can be attributed to galaxies involved in some stage of a major merger (Fig. 11). The remaining ~40% of the IR background from LIRG/ULIRGs is likely to come predominantly from active, isolated gas-rich star-forming spirals, with some contribution from minor mergers.

If we exclude visually classified mergers, the close pair/merger contribution to the IR density is ~38%, in good agreement with Lin et al. (2007), who estimate a moderate contribution from interacting and merging systems of $\lesssim$36%. It must be noted, however, that neither Lin et al. (2007) nor this work have considered the contribution from minor mergers and therefore these are lower limits.

6.1. *Star Formation in Mergers and Interactions*

An important and highly debated question is, how important are galaxy mergers in understanding the dramatic decline of the

CSFR density from $z \sim 1$ to the present day? It has been well established that mergers and interactions can induce violent bursts of star formation (Schweizer 1982; Barton et al. 2000; Mihos & Hernquist 1996; Cox et al. 2006). So, to investigate this contribution, we derived the star foramtion rate (SFR) for our 24 μm detected close pairs and mergers, using their $L_{\rm IR}$. The infrared luminosity of a galaxy is a star formation rate tracer that is unaffected by the extinction of dust. The dominant heat source of most dusty, high-opacity systems, such as LIRGs and starbursts, is stellar radiation from young stars. In these types of systems the $L_{\rm IR}$ can be converted into a SFR using the calibration of Kennicutt (1998), $\mathrm{SFR_{IR}} = 4.5\times10^{-44} L_{\rm IR}(\mathrm{erg\ s^{-1}})$, where $L_{\rm IR}$ is the integrated luminosity from 8 to 1000 μm as determined in § 6.

We estimated the contribution that mergers and interactions above $L_{\rm IR} \geq 10^{11}\ L_{\odot}$ make to the SFR density at $z \sim 1$ in two ways. The first is simply to consider their contribution to the $L_{\rm IR}$ density, which is a star formation tracer. Section 6 determined that mergers and interactions at $z \sim 1$ (above $L_{\rm IR} \geq 10^{11}\ L_{\odot}$) are responsible for 40%–60% of the IR luminosity density. Using the results of Le Floc'h et al. (2005), which showed that $z \geq 0.7$ LIRGs produce ~70% of the star formation rate density, we can infer that mergers and interactions in the LIRG/ULIRG phase would be responsible for ~30%–40% (0.6×70%) of the SFR density at $z \sim 1$, since IR activity traces dusty star formation.

The second, more detailed, approach utilizes the SFR density directly arising from our sample of mergers and interactions. At $1.0 \leq z \leq 1.3$, we find that 59% (12 close pairs and 17 later stage mergers) of galaxies detected at 24 μm are involved in some stage of an interaction or merger. In this same redshift range, our sample is insensitive to galaxies with IR luminosities $\leq 10^{11.5}$. To correct for this, we derived a scaling factor (~7) simply by comparing the number of observed objects of a given $L_{\rm IR}$ in a specific redshift range to the number expected from models (Lagache et al. 2004). However, to go any further, we must assume that our spectroscopic sample is representative of this population at ~1, and by all accounts this appears to be true. Using the derived pair fraction, we can then infer the total number of major mergers and interactions occurring (fulfilling our criteria) in a given volume and $L_{\rm IR}$ limit. The lower limit of the SFR density at $z \sim 1$ from merging and interacting galaxies is found to be $0.066\ M_{\odot}\ \mathrm{yr^{-1}\ Mpc^{-1}}$. Using the extinction-corrected Lilly-Madau plot ($0.1585\ M_{\odot}\ \mathrm{yr^{-1}\ Mpc^{-1}}$ at $z = 1$; Thompson et al. 2001), we find that mergers and interactions are responsible for at least 42% of the SFR density at $z \sim 1$ (assuming mergers contribute 60% of the IR density). Both approaches are in good agreement and are only a lower limit, since objects flagged as AGNs were not considered, even though some of their $L_{\rm IR}$ is a result of star formation, and minor mergers that have also been shown to induce bursts of star formation were not included.

These results have interesting implications for the physical mechanisms that drive the decline in the CSFR density from $z \sim 1$ to the present day. They suggest that when all stages of the merger process are considered (premerger to later stage merger), major interactions and mergers contribute close to half of the $z \sim 1$ SFR density, and the decline in the number of 24 μm detected mergers/interactions is a significant, but perhaps not the primary, driver for the decline in the CSFR. This conclusion differs in interpretation from Bell et al. (2005), Melbourne et al. (2005), Wolf et al. (2005), Lin et al. (2007), and Lotz et al. (2006), which generally suggest that the evolution of the merger rate is not a significant underlying cause of the decline in the CSFR, but rather that a strong decrease in the SFR of morphologically undisturbed spiral galaxies is the dominant mechanism. Their results do not preclude the possibility that their "star-forming (undisturbed) disks" could be in widely separated pairs, and when we only consider quantitatively defined morphological mergers, our results are consistent with theirs, stressing the importance of considering the merger process in its entirety. It must also be mentioned that we are probing to higher redshifts than Bell et al. (2005), who found that major galaxy mergers account for ≤30% of the IR luminosity density at $z \sim 0.7$, consistent with our findings of 35% at that redshift. Our results also agree that at $z \sim 0.7$ isolated, undisturbed spiral galaxies are a primary contributor; however, the influence shifts to interactions and mergers at $z \sim 0.7$.

Our findings point to an increased importance of MIPS-bright interactions and mergers to the IR luminosity density and SFR density at $z \sim 0.7$. This conclusion is not weakened by the small statistics of the $z > 1$ bin. Figure 11 shows the IR luminosity density contribution from interactions/mergers at $z \sim 0.7$ to be ~37% and 52% at $z \sim 0.9$, reinforcing this increasing trend.

7. DISCUSSION

Using a spectroscopic sample of field galaxies from the ACS component of the FLS and dividing it into two subsets, those with a 24 μm detection (above 0.1 mJy) and those without (or below), we identified optically merging/interacting systems via close pair statistics and morphological methods. We find that roughly 25% of galaxies emitting at 24 μm have a close companion at $z \sim 1$, while at $z \sim 0.5$ only ~11% are in pairs. In contrast, those undetected at MIPS 24 μm showed a pair fraction consistent with zero at all redshifts ($0.2 \leq z \leq 1.3$). On average, MIPS 24 μm galaxies are 5 times more likely than non-MIPS sources to have a close companion over $0.2 \leq z \leq 1.3$. When the samples are combined (regardless of 24 μm flux), we find pair fractions consistent with previous studies (Lin et al. 2004; Bundy et al. 2004), showing little evolution with redshift.

An important and open question is the cause of star formation in LIRG galaxies at high z. Some morphological studies have suggested that, since at least half of the LIRG galaxies exhibit disk-dominated morphologies (Bell et al. 2005; Lotz et al. 2006) at $z \geq 0.7$ and low nonevolving merger fractions (Lotz et al. 2006), the driver of IR activity in high-z LIRGs is ongoing star formation from isolated gas-rich spirals, not merger or interaction induced. One bias of *HST* morphological studies involving the identification of merging/intereacting systems is the limitation of detecting low surface brightness features, such as tidal tails caused by close interactions, which can lead to an underestimate of the importance of mergers in the evolution of galaxies at $z < 1$. Ultimately, both close pair and morphological techniques must be applied and considered to obtain a complete major merger timeline. Our analysis is the first to probe merger rate evolution combining close pairs and later stage mergers while considering the IR activity of these systems.

We find that close pair statistics, visually classified mergers, and those identified via quantitative CAS parameters all showed similar evolution in their merger rates. Fitting the merger rate evolution function $\mathcal{R}(z) \propto (1+z)^m$ for 24 μm detected mergers above 0.1 mJy, we find $m = 2.12 \pm 0.93$. This result agrees with previous claims of an increase ($m \geq 2$) of the merger rate out to $z \sim 1$ (Patton et al. 1997, 2000; Le Fèvre et al. 2000; Conselice et al. 2003b; Cassata et al. 2005). However, this evolution is not seen when IR-faint (<0.1 mJy) mergers are included, suggesting that it is the LIRG-merger population that is evolving with redshift.

The mid-IR emission of LIRGs is indicative of dust-enshrouded star formation (and some AGN activity), and at $z \geq 0.7$ they dominate the IR luminosity density and in turn the volume-averaged

star formation rate density at $z \sim 1$. We estimate that close galaxy pairs are responsible for ~27% of the IR luminosity density resulting from star formation at $z \sim 1$, while later stage mergers contribute ~35%. This implies that 40%–60% of the infrared luminosity density at $z \sim 1$ can be attributed to galaxies involved in some stage of a major merger, indicating that merger-driven star formation is responsible for 30%–40% of the star formation density at $z \sim 1$. This value is a lower limit, since minor mergers and interactions/mergers with an AGN were not considered. Ultimately, our findings suggest that interactions and mergers of LIRG phase galaxies play an increasingly important role in both the IR luminosity and SFR density from $z \geq 0.7$ out to $z \sim 1.3$ and are vital to our understanding of the evolution and mass assembly of luminous IR galaxies.

We would like to thank H. Shim, M. Im, R. Chary, and C. Borys for their contributions to this work, V. Charmandaris for useful suggestions, and the anonymous referee for valuable comments that improved the clarity of the paper. This work is based on observations made with the *Spitzer Observatory*, which is operated by the Jet Propulsion Laboratory, California Institute of Technology, under NASA contract 107. Support for this work was provided in part by the Spitzer Graduate Student Fellowship program and an Ontario Graduate Scholarship in Science and Technology. The authors wish to recognize and acknowledge the very significant cultural role and reverence that the summit of Mauna Kea has always had within the indigenous Hawaiian community. We are most fortunate to have the opportunity to conduct observations from this mountain.

REFERENCES

Abraham, R. G., Tanvir, N. R., Santiago, B. X., Ellis, R. S., Glazebrook, K., & van den Bergh, S. 1996a, MNRAS, 279, L47
Abraham, R. G., van den Bergh, S., Glazebrook, K., Ellis, R. S., Santiago, B. X., Surma, P., & Griffiths, R. E. 1996b, ApJS, 107, 1
Abraham, R. G., van den Bergh, S., & Nair, P. 2003, ApJ, 588, 218
Barnes, J. E. 2004, MNRAS, 350, 798
Barton, E. J., Geller, M. J., & Kenyon, S. J. 2000, ApJ, 530, 660
Bell, E. F., et al. 2005, ApJ, 625, 23
Bertin, E., & Arnouts, S. 1996, A&AS, 117, 393
Bundy, K., Fukugita, M., Ellis, R. S., Kodama, T., & Conselice, C. J. 2004, ApJ, 601, L123
Burkey, J. M., Keel, W. C., Windhorst, R. A., & Franklin, B. E. 1994, ApJ, 429, L13
Carlberg, R. G., Pritchet, C. J., & Infante, L. 1994, ApJ, 435, 540
Carlberg, R. G., et al. 2000, ApJ, 532, L1
Cassata, P., et al. 2005, MNRAS, 357, 903
Chary, R., & Elbaz, D. 2001, ApJ, 556, 562
Choi, P. I., et al. 2006, ApJ, 637, 227
Conselice, C. J. 1997, PASP, 109, 1251
———. 2003, ApJS, 147, 1
———. 2006, ApJ, 638, 686
Conselice, C. J., Bershady, M. A., Dickinson, M., & Papovich, C. 2003a, AJ, 126, 1183
Conselice, C. J., Bershady, M. A., & Jangren, A. 2000, ApJ, 529, 886
Conselice, C. J., Blackburne, J. A., & Papovich, C. 2005, ApJ, 620, 564
Conselice, C. J., Chapman, S. C., & Windhorst, R. A. 2003b, ApJ, 596, L5
Conselice, C. J., Gallagher, J. S., III, & Wyse, R. F. G. 2002, AJ, 123, 2246
Cox, T. J., Jonsson, P., Primack, J. R., & Somerville, R. S. 2006, MNRAS, 373, 1013
Dale, D. A., Helou, G., Contursi, A., Silbermann, N. A., & Kolhatkar, S. 2001, ApJ, 549, 215
Dasyra, K. M., et al. 2006, ApJ, 638, 745
Efron, B., &Tibshirani, R. 1986, Stat. Sci., 1, 54
Elbaz, D., Cesarsky, C. J., Chanial, P., Aussel, H., Franceschini, A., Fadda, D., & Chary, R. R. 2002, A&A, 384, 848
Fadda, D., Jannuzi, B. T., Ford, A., & Storrie-Lombardi, L. J. 2004, AJ, 128, 1
Fadda, D., et al. 2006, AJ, 131, 2859
Fazio, G. G., et al. 2004, ApJS, 154, 10
Kennicutt, R. C., Jr. 1998, ARA&A, 36, 189
Lacy, et al. 2004, ApJS, 154, 166
———. 2005, ApJS, 161, 41
Lagache, G., et al. 2004, ApJS, 154, 112
Lavery, R. J., Remijan, A., Charmandaris, V., Hayes, R. D., & Ring, A. A. 2004, ApJ, 612, 679
Le Fèvre, O., et al. 2000, MNRAS, 311, 565
Le Floc'h, E., et al. 2005, ApJ, 632, 169
Lin, L., et al. 2004, ApJ, 617, L9
———. 2007, ApJ, in press (astro-ph/0607272)
Lotz, J. M., et al. 2006, ApJ, submitted
Melbourne, J., Koo, D. C., & Le Floc'h, E. 2005, ApJ, 632, L65
Mihos, J. C., & Hernquist, L. 1996, ApJ, 464, 641
Patton, D. R., Carlberg, R. G., Marzke, R. O., Pritchet, C. J., da Costa, L. N., & Pellegrini, P. S. 2000, ApJ, 536, 153
Patton, D. R., Grant, J. K., Simard, L., Pritchet, C. J., Carlberg, R. G., & Borne, K. D. 2005, AJ, 130, 2043
Patton, D. R., Pritchet, C. J., Yee, H. K. C., Ellingson, E., & Carlberg, R. G. 1997, ApJ, 475, 29
Patton, D. R., et al. 2002, ApJ, 565, 208
Rieke, G. H., et al. 2004, ApJS, 154, 25
Sanders, D. B., Soifer, B. T., Elias, J. H., Madore, B. F., Matthews, K., Neugebauer, G., & Scoville, N. Z. 1988, ApJ, 325, 74
Schweizer, F. 1982, ApJ, 252, 455
Thompson, R. I., Weymann, R. J., & Storrie-Lombardi, L. J. 2001, ApJ, 546, 694
Shim, H., Im, M., Pak, S., Choi, P., Fadda, D., Helou, G., & Storrie-Lombardi, L. 2006, ApJS, 164, 435
Wolf, C., et al. 2005, ApJ, 630, 771
Xu, C. K., Sun, Y. C., & He, X. T. 2004, ApJ, 603, L73
Yee, H. K. C., & Ellingson, E. 1995, ApJ, 445, 37
Zepf, S. E., & Koo, D. C. 1989, ApJ, 337, 34